*Recent Trends in Sturctural Integrity Assessment, Eds.: V.R. Ranganath, S. Tarafder, A. Bahadur, 18-19 January 2001, National Metallurgical Laboratory, Jamshedpur, India, pp. 46-57.*

# Catastrophic Carburisation in Petrochemical Industry

**S. R. SINGH**

*National Metallurgical Laboratory, Jamshedpur - 831 007*

## ABSTRACT

This paper reports catastrophic carburisation (metal dusting corrosion) of radiant tube of a Pacol reactor which has undergone service life of 67,000 hours in a petrochemical plant. The 6" dia. tube conforms to Sch. 40 of ASTM A335-P11 (1.25Cr-0.5Mo steel). The failure of tubes occurred due to non-uniform thinning of tube wall leading to fracture. The failed tube was investigated by x-ray diffraction phase analysis, scanning electron microscopy, energy dispersive spectroscopy and optical microscopy for characterisation of reaction products. The inner wall of tube surface contained wustite, magnetite, $Cr_2C$, $M_{23}C_6$, rounded iron metal particles and irregular shaped carbon soot.

The presence of wustite in scale deposit revealed that the tube temperature was above or around 600°C, while the absence of hematite, which grow in presence of water vapour and thermodynamically unstable to high reducing gas atmosphere, was consistent with the atmospheric condition in the tube. The structural identification of $Cr_2C$ and $M_{23}C_6$ phases and morphological features near the base metal of inside surface revealed highly carburised inner tube metal surface. The wall thinning in thicker region of the tube is in the form of rounded pits, whereas in thinner region of tube, metal loss in the form of uniform localised thinning was encountered. The carbon soot deposits were mostly on the thicker wall region. All these observations indicate that the metal wastage was due to carburising condition.

## INTRODUCTION

In petrochemical industries, the life controlling conditions are usually governed by; (i) creep rupture damage, and (ii) thermal shock. In addition to creep damage, and the effects of the higher temperatures, the life of coil alloys is also dependent on; (i) carburisation, (ii) oxidation, (iii) thermal shock due to cycling. The creep damage is most important for materials applications at high temperatures. At the same time, the effect of carburisation on creep resistance and ductility depend on the conditions of carburisation [1,2]. In a low carbon material, the carburisation at relatively low temperatures gives rise to fine precipitation at grain boundaries which increases the creep resistance [1]. However, if such material is carburised at high temperature and large blocky carbides are formed, the rupture time is decreased and rupture strain is high. Thus carburisation does not cause the creep behavior of materials to deteriorate if the carbon content attained is not too high.

Carburisation is observed in several industrial processes under carbonaceous atmosphere at high temperature. Carbon is transferred from gas atmosphere to the alloy matrix, and internal carbides are formed. Usually, the alloys are protected against carburisation by an oxide layer (magnetite or spinel) barrier against carbon ingress. The oxide scale breakdown occurs by graphite (coke) in and on the scale [3]. This mechanism leads mechanical failure of protective oxide scales in cracking tubes in petrochemical plant. Metal dusting is a catastrophic carburisation [4,5] which is a particularly aggressive form of high temperature corrosion of Fe, Co and Ni based alloys by a sulfur-free mixtures of hydrocarbon leading to internal carbide formation of alloying elements and the development of thermodynamically metastable carbides of the base metal. These metastable carbides decompose into a powder consisting of carbon and metal. Therefore, this carburisation corrosion phenomenon is often referred to as metal dusting where corrosion products consist of dust of metals, metal carbides, oxides and carbon. This is a form of rapid metal wastage in carbonaceous gas streams e.g., $CO/CO_2$, hydrocarbons etc., generally in the temperature range 400 - 800°C. The wastage is often in the form of rounded pits, but in some cases metal loss in the form of uniform thinning is encountered, particularly where gas velocities are high. The surface from which metal is lost are generally carburised, in fact, in almost every case where wastage is of the pitting type, though it is often more difficult to detect carburisation if the wastage is of the uniform variety in high velocity gas stream. This phenomenon is dependent on large number of factors, *i.e.*, gaseous phase composition, temperature, pressure, alloy type and component shape. Sometimes minor changes in process condition can cause onset or arrest of metal dusting or move the attack to another location. The common characteristics of catastrophic carburisation (metal dusting corrosion) are in summarised Table 1.

*Table 1: Characteristics of catastrophic carburisation.*

| | |
|---|---|
| *Environment* | Carburising and reducing gas phase, with or without oxygen-containing components. |
| *Temperature range* | 400 - 800°C. |
| *Form of deterioration* | Localized or general pitting, or more general overall surface wastage where the surface/subsurface are carburised. |
| *Corrosion products* | Loosely adherent dust or powder consisting of carbon, metal, metal carbides and metal oxides. |

Another form of high temperature corrosion of Mo-containing steels encountered in petroleum refining and petrochemical industries is catastrophic oxidation [6] which generally occurs in stagnant conditions. Certain oxides of alloy containing Mo, W, and V forms low melting eutectics with other oxides present in the scale and this low melting constituents acts in such a way as to render the scale more pervious. The data from Mo-containing steel shows that certain mixed oxide system based on $MoO_2$, $MoO_3$, $Cr_2O_3$, NiO, $Fe_2O_3$ have melting points in the range of 725 - 800°C. Also $Na_2O$

from insulation and refractories can give rise to $Na_2O$ - $MoO_3$ mixture melting as low as 550°C.

In the present case, a detailed x-ray diffraction analysis, scanning electron microscopy (SEM) and energy dispersive analysis of x-ray (EDAX) studies of thin layer/deposit inside the failed 6" dia. Sch. 40 ASTM A335-P11 reactor tubes have been made to characterise the reaction products. The alloy composition of Pacol reactor tube conforms to 1.25Cr-0.5Mo steel. The tubes served for about 67,000 hours. In the process the N-paraffin hydrocarbon mixed with recycled hydrogen having $H_2$/HC ratio of 6:1 goes into Pacol reactor in vapor state. The service conditions are summarised Table 2.

*Table 2: Service conditions of the failed tube*

| | |
|---|---|
| *Alloy composition:* | Conforms to ASTM-A335-P11 (1.25Cr-0.5Mo steel). |
| *Dimension of tube:* | 168.3mm OD x 7.2mm thick. |
| *Temp. of outer surface* | Heater inside temp. is 1200°C near burner combustion zone and is gradually comes down to about 600 - 650°C in convection zone of heater. But frequently observed skin temperature is 700°C. |
| *Atmosphere outside tube* | Hot air due to combustion of fuel at normal atmospheric pressure. |
| *Fluid inside tube* | N-Paraffin hydrocarbon mixed with recycled hydrogen having $H_2$/HC ratio 6:1. |
| *Inlet temp. of hydorcarbon* | 380°C. |
| *Design inlet temp. & pressure* | 419°C, 2.1kg/cm$^2$. |
| *Outlet temp. of hydrocarbon* | 490°C. |
| *Design outlet temp. & pressure* | 593°C, 7kg/cm$^2$. |
| *Pressure inside tube* | 2kg/cm$^2$. |

## Experimental Procedures and Results

### *Visual examination*

The failed tube was cut in transverse direction. A photograph of the tube is shown in Fig. 1. Wall thickness of tube was non-uniform having maximum thickness of 6.8 mm (hereafter referred as region "A") and minimum thickness of 3.6 mm (hereafter referred as region "B"). These two regions were diametrically opposite and outer

diameter across it was 170 mm while outer diameter perpendicular ("CD") to it was 168 mm. Inner surface of the tube has dull black appearance with sooty deposits. These dimensional measurements showed that the tube had undergone 1% expansion in direction "AB", where wall thinning was maximum while there was no appreciable deformation perpendicular to "AB", *i.e.*, "CD". These observations indicate that the failure would have taken place due to non-uniform wall thinning.

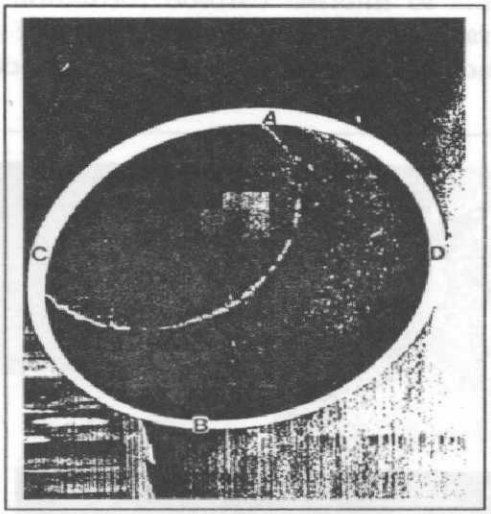


*Fig. 1: A photograph of transverse section of tube showing maximum and minimum wall thickness regions marked "A" and "B" respectively. Non-uniform wall thinning can be noticed.*

### *Optical metallography*

The optical metallography of transverse section of the tube revealed that the matrix has usual microstructure consisting of ferrite and tempered bainite. A typical microstructure is shown in Fig. 2a whereas Figs. 2b & 2c showed matrix/scale interface of outer and inner tube surfaces respectively. The scale at outer tube surface (Fig. 2b) is thicker, compact and undamaged with no significant changes in subsurface matrix microstructure, while the scale at inner tube surface (Fig. 2c) showed thinner/broken scale with altered subsurface microstructure of base metal. The thin scale in Fig. 2c was out of focus. These observations indicate that there was breakdown of protective scale which lead to the alteration of subsurface matrix microstructure at the inner wall of tube.

### *Scanning electron microscopy & microanalysis by EDAX*

Transverse section metallography samples from region "A" undergone minimum wall thinning were examined by SEM. All the microstructures were recorded in secondary electron imaging mode, although, backscattered images were also analyzed for better perception. Fig. 3a showed typical ferrite and tempered bainite microstructure of the matrix far away from both the surfaces. The inner tube surface/matrix microstructure (Fig. 3b) revealed the duplex nature of oxide scale

consisting of thin inner wustite layer and thick outer magnetite/spinel layer. The outer magnetite scale layer is broken while the inner wustite scale layer is compact. If the composite scale layer is broken in service, ingress of carbon to subsurface region lead to general carburisation manifested by initiation of pitting with thick continuous network of grain boundary carbides as well as fine intragranular carbides (Fig. 3c). A comparison of Fig. 3a with Figs. 3b &c showed an increase in intergranular as well as intragranular carbide precipitates in the subsurface region of the inner tube wall. This shows that, carburisation leads to internal carbide formation due to relatively high inward diffusion of carbon rather than outward diffusion of carbide forming metal atoms. Figure 3d showed another example of pitting after complete breakdown of scale.

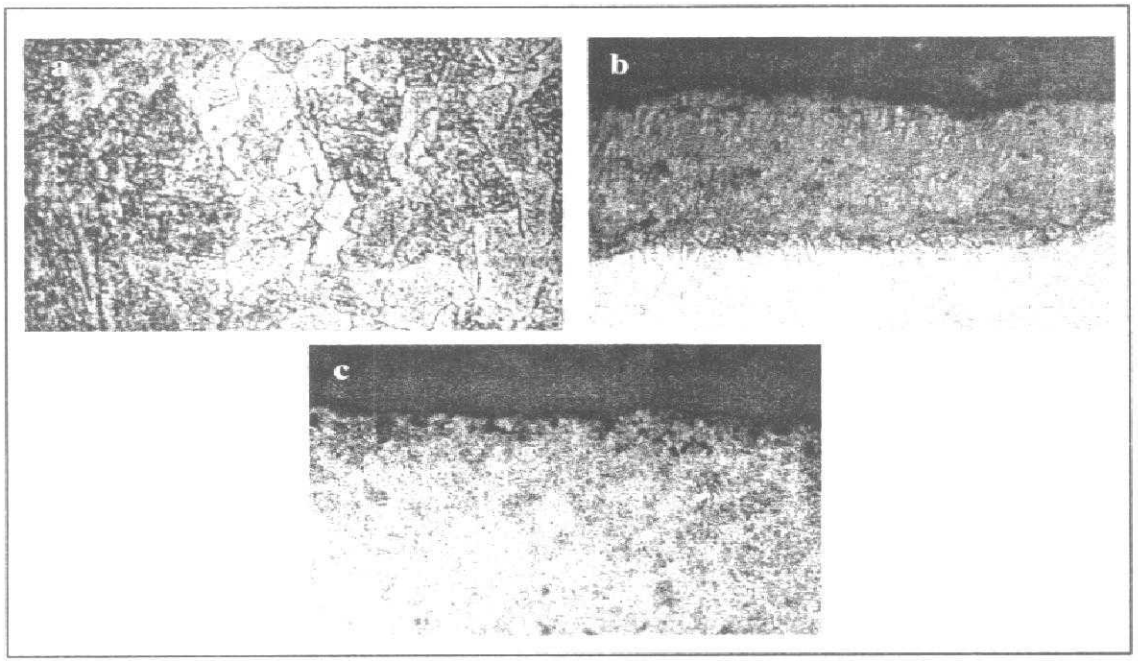


*Fig. 2: Optical micrographs of transverse section of tube showing, (a) ferrite and tempered bainite in the matrix, (b) outer tube scale interface, (c) inner tube scale interface.*

The longitudinal section of inner tube surface from region "A" having sooty deposits was also examined in as received condition. Figure 4a revealed that the deposits consist of spherical particles dispersed on irregular shaped particles/soot, which is devoid of any whisker growth (Fig. 4b).

Transverse section metallography samples from region "B" were also examined. SEM micrographs from unaltered matrix and subsurface region of inner tube wall are shown in Fig. 5a & b respectively. Coarsening of grain boundary precipitates as well as increase in number density of precipitates in the subsurface region has taken place. Also the pitting in region "B" is absent. This indicates that the uniform metal wastage

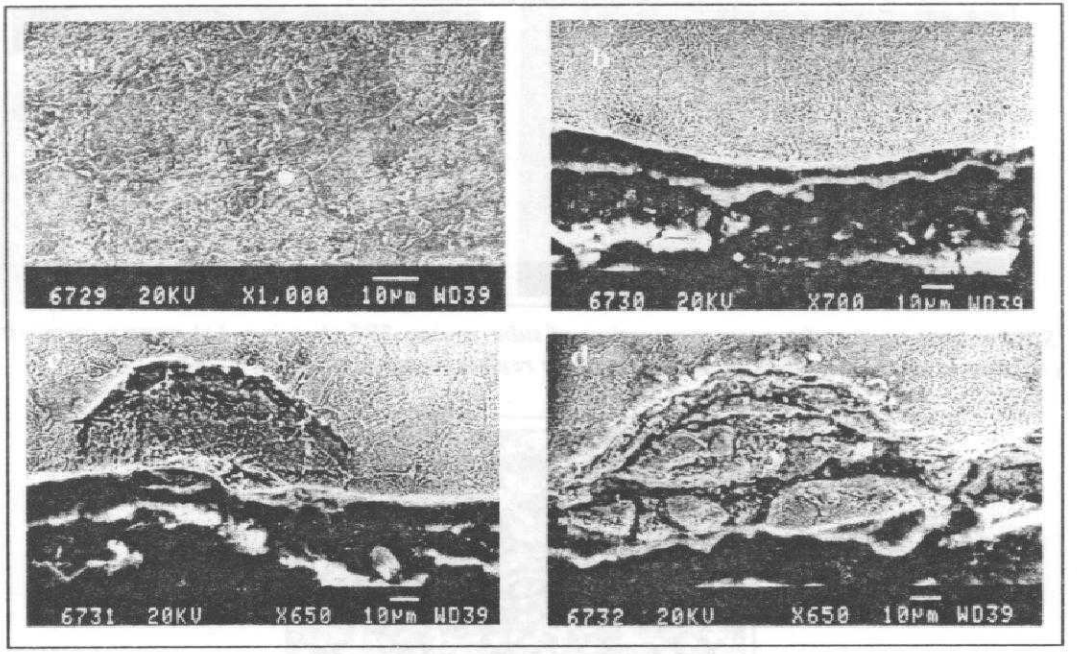


*Fig. 3: SEM micrographs of transverse section of tube region "A" showing, (a) ferrite-tempered bainite microstructure of the matrix, (b) inner tube surface-matrix interface, (c) pitting initiation at inner tube surface, (d) pitting after complete breakdown of scale.*

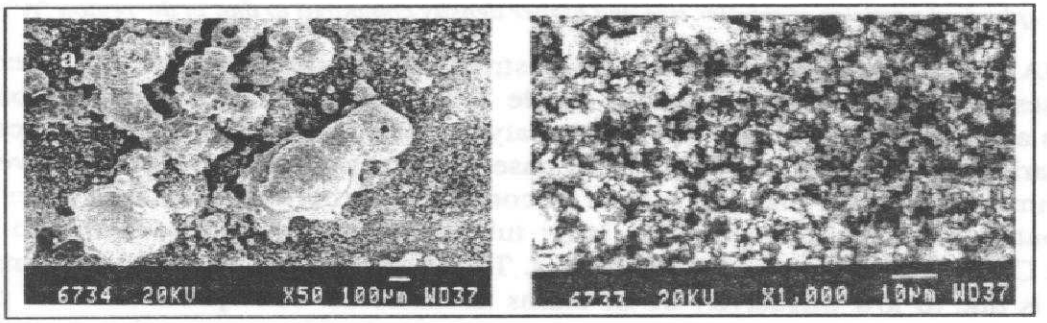


*Fig. 4: SEM micrographs of as received longitudinal section of inner tube surface of region "A" revealing, (a) spherical particles dispersed on irregular shaped particles, (b) higher magnification of irregular shaped particles.*

by catastrophic carburisation was operative in the region "B". SEM micrograph (Fig. 6) from as received longitudinal surface showed higher number density and smaller size of spherical particles are dispersed on the surface while there is a significant reduction in irregular sooty deposits in region "B" (compare it with Figs. 4a & b recorded from region "A").

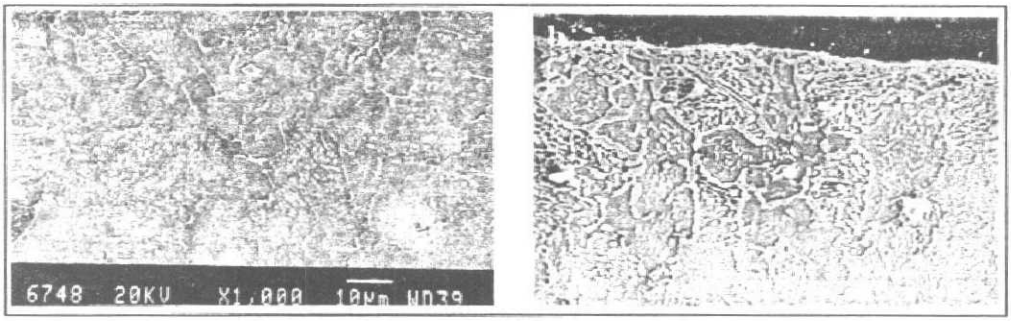


*Fig. 5: SEM micrographs of transverse section of tube region "B" showing, (a) matrix microstructure, (b) altered microstructure in the subsurface region (inner wall of the tube).*

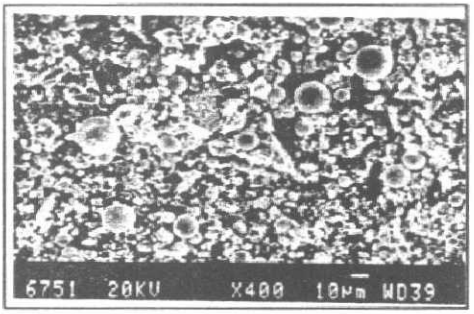


*Fig. 6: SEM micrograph of as received longitudinal section of inner tube surface of region "B" showing spherical particles of smaller size and higher density compared to that in the region "A".*

EDAX microanalyses of various microstructural constituents have been performed to assess the elemental partitioning. Table 3 showed the EDAX compositional data which are compared with wet chemical analysis and ASTM A335-P11 specification. A comparison of composition (EDAX) of base metal with carburised zone showed some enrichment of Mo, Cr and decrease of Si content in carburised zone. The inner wustite and outer magnetite scales on the inner tube surface are enriched with Mo and Si, while Cr content decreased in both scales. The lesser amount of Cr in outer magnetite scale is due to low diffusivity of Cr atoms in the scale. The spherical metal particles are also enriched with Mo but Cr content is decreased with respect to base metal.

### *X-ray diffraction studies*

X-ray diffraction studies were made with Siemens D-500 diffractometer on samples from inside surfaces of the tube. Diffractogram of samples from region "A" of inner tube surface was recorded with $CoK_\alpha$ radiation. The phases were identified with the help of ASTM Powder Diffraction Files. In the diffractogram from region "A", peaks corresponding to phases; ferrite, wustite, magnetite, $Cr_2C$, $M_{23}C_6$ were characterised. The ferrite peaks originated from base metal as well as spherical metal particles, which were formed due to carburisation of base metal. Diffraction peaks are numbered in

serial order with decreasing interplanar spacings ($d$-values). The observed $d$-values and $2\theta$-values of corresponding phases alongwith their indices are collated in Table 4.

*Table 3: Chemical composition (wt.%) of various regions of the failed tube.*

| *Area* | *Cr* | *Mo* | *Si* | *Mn* | *C* | *S* | *P* | *Fe* | *Remarks* |
|---|---|---|---|---|---|---|---|---|---|
| *Base metal* | 1.48 | 0.61 | 0.87 | 0.38 | 0.14 | 0.014 | 0.003 | 96.50 | Chem. analysis |
| *A335-P11* | 1-1.5 | 0.44-0.65 | 0.5-1.0 | 0.3-0.6 | 0.05-0.15 | 0.025 (max.) | 0.025 (max.) | balance | Specs. |
| *Base Metal* | 1.54 | 0.54 | 0.57 | 0.84 | * | * | * | 96.51 | EDAX |
| *Carburised zone* | 1.60 | 0.74 | 0.33 | 0.84 | * | * | * | 96.48 | EDAX |
| *Inner scale* | 1.08 | 3.92 | 3.34 | 0.46 | * | * | * | 91.21 | EDAX |
| *Outer scale* | 0.24 | 2.32 | 1.21 | 0.44 | * | * | * | 95.79 | EDAX |
| *Spherical particles* | 0.47 | 1.18 | 0.78 | 0.37 | * | * | * | 97.20 | EDAX |

* Not detected by EDAX.

Wustite forms above 570°C and Cr, Mo addition raises it to 600°C. Therefore, the presence of wustite in the scale indicates that the region "A" of the tube had experienced temperature in excess of 600°C. The absence of hematite, which grow in presence of water vapor and thermodynamically unstable to high reducing gas atmosphere, was consistent with the atmospheric condition in the tube. The x-ray diffractogram from region "A" also showed the increased background, which increases with $2\theta$. This is due to Compton scattering from amorphous low atomic weight elements/phases. In the amorphous bodies, however the incoherent radiation may form an important fraction of total scattered radiation, particularly, for large scattering vectors. The intensity of Compton scattering is given by,

$$I_{\text{Compton}} = Z - \Sigma f_j^2 \qquad \cdots (1)$$

where $Z$ is atomic number and f is the atomic scattering factor of the element. For $\theta = 0$, $f$ equals to $Z$ and falls of as $\theta$ increases. Also, as atomic number of element increases, $f^2$ increases more rapidly. Thus Compton scattering decreases in intensity as atomic number of scatterer increases. Therefore increases background intensity with $2\theta$ is due to presence of low atomic number species in the sample, *i.e.*, carbon in the present case. The diffraction data from diffractogram of sample from region "B", recorded with $FeK_\alpha$ radiation, are collated in Table 5. This sample showed the peaks corresponding to ferrite, magnetite, $Cr_2C$ and $M_{23}C_6$ while wustite peaks are absent. The overall relative volume fraction of all the phases in both the regions are at variance. The background intensity did not vary with scattering angle $2\theta$. With the reasoning provided above, It may be concluded that the carbon soot is negligibly small in this region ("B"). The unidentified peaks marked by "*" in Tables 4 & 5 are

probably artifacts, because they did not match with the stable or metastable phases expected from phase diagram; $Cr_7C_3$, $Cr_3C_2$, $Fe_7SiO_7$, $FeCr_2O_4$, $FeCr_2S$, $Cr_2S_3$, $Cr_3S_4$, CrS, $Fe_2O_3$, $\gamma$-Fe, Cr, Mo, Si, besides the identified phases.

*Table 4: X-ray diffraction data obtained from sample region "A".*

| *Sl. No* | *2θ (degree)* | *Observed interplanar spacings (Å)* | *Corresponding phases and index of plane* |
|---|---|---|---|
| *1* | 20.978 | 4.9171 | Magnetite (111) |
| *2* | 34.780 | 2.9950 | Magnetite (220) |
| *3* | 41.098 | 2.5502 | Magnetite (311) |
| *4* | 42.090 | 2.4927 | Wustite (111) |
| *5* | 43.689 | 2.4057 | $Cr_2C$ (100) |
| *6* | 47.170 | 2.2372 | $Cr_2C$ (002) |
| *7* | 49.150 | 2.1524 | Wustite (200) |
| *8* | 50.111 | 2.1137 | $Cr_2C$ (101) |
| *9* | 50.886 | 2.0836 | Magnetite (400) |
| *10* | 51.998 | 2.0420 | Ferrite (110) |
| *11* | 53.414 | 1.9917 | * |
| *12* | 56.694 | 1.8852 | $M_{23}C_6$ (440) |
| *13* | 57.392 | 1.8642 | * |
| *14* | 60.624 | 1.7736 | $M_{23}C_6$ (600) |
| *15* | 65.790 | 1.6482 | $Cr_2C$ (102) |
| *16* | 67.018 | 1.6214 | Magnetite (511) |
| *17* | 68.210 | 1.5964 | * |
| *18* | 71.882 | 1.5250 | Wustite (220) |
| *19* | 73.896 | 1.4892 | Magnetite (440) |
| *20* | 76.935 | 1.4390 | Ferrite (200) |
| *21* | 84.660 | 1.3293 | Magnetite (620) |
| *22* | 87.200 | 1.2980 | Wustite (311) |
| *23* | 92.100 | 1.2433 | Wustite (222) |
| *24* | 99.440 | 1.1733 | Ferrite (211) |
| *25* | 100.500 | 1.1640 | $Cr_2C$ (201) |

*unidentified artifact peaks

*Table 5: X-ray diffraction data obtained from sample region "B".*

| *Sl.No* | *2θ (degree)* | *Observed Interplanar spacings (Å)* | *Corresponding phases and Index of plane* |
|---|---|---|---|
| *1* | 37.790 | 2.9912 | Magnetite (220) |
| *2* | 44.680 | 2.5484 | Magnetite (311) |
| *3* | 47.608 | 2.3999 | $Cr_2C$ (100) |
| *4* | 51.490 | 2.2300 | $Cr_2C$ (002) |
| *5* | 54.480 | 2.1162 | $Cr_2C$ (101) |
| *6* | 55.547 | 2.0787 | Magnetite (400) |
| *7* | 56.759 | 2.0379 | Ferrite (110) |
| *8* | 58.341 | 1.9873 | * |
| *9* | 61.949 | 1.8821 | $M_{23}C_6$ (440) |
| *10* | 62.747 | 1.8606 | * |
| *11* | 66.394 | 1.7692 | $M_{23}C_6$ (600) |
| *12* | 73.489 | 1.6191 | Magnetite (511) |
| *13* | 74.833 | 1.5942 | * |
| *14* | 81.236 | 1.4879 | Magnetite (440) |
| *15* | 84.763 | 1.4370 | Ferrite (200) |
| *16* | 93.460 | 1.3303 | Magnetite (620) |
| *17* | 105.225 | 1.2191 | Magnetite (444) |
| *18* | 111.451 | 1.1722 | Ferrite (211) |
| *19* | 112.950 | 1.1619 | $Cr_2C$ (201) |

*unidentified artifact peaks

## DISCUSSION

For carburisation encountered in industrial applications, the rate is restricted by the presence of oxide scale formed on the alloy surface. Under such conditions, provided temperature and environment don't vary with time, the carburisation rate will be constant. Linear carburisation kinetics of this type has been found for wide range of high temperature alloys exposed to 900°C. If no surface oxide is present on the alloy and surface reaction rates are sufficiently high, the rate of carburisation will be controlled by diffusion and precipitation process in the alloy matrix. Under such conditions, the carburisation kinetics is essentially parabolic. The high carburisation rates would be expected in chemical plant when surface oxide scale have been broken down, *e.g.*, due to severe overheating and duration of the exposure under such

conditions would probably be short in comparison with the long term steady state carburisation expected under normal operating condition.

The reaction products of catastrophic carburisation (metal dusting corrosion) are found to be carbon, carbides and oxides, interspersed with metal particles which is poor in Cr. These corrosion products are loosely adherent and can be easily eroded, which lead to, further pitting or uniform thinning in the presence of carburising conditions. High temperature carburisation involves following kinetic steps: (i) transport in the gas atmosphere by gas flow or gaseous diffusion; (ii) Carbon transfer to the metal phase by phase boundary reaction which are reaction of the gas molecules on the surface, leading to carbon atoms; (iii) inward diffusion of dissolved carbon in the metal; (iv) reaction of carbon with carbide forming elements in the alloy interior, and diffusion of carbide forming elements to precipitates.

In carburisation of materials without protective oxide layer, step (i) in the transport/diffusion of carbonaceous molecules in the boundary layer above the metal surface. If a more or less dense oxide layer is present, the carbonaceous molecule must diffuse to the oxide-metal interface by pores or cracks in the oxide layer. Because of immeasurably low solubility of carbon in oxides, permeation in carbon atoms through oxide layers is not possible [7]. Cracks are also formed in the oxide layers by creep, fatigue or thermal cycling. The oxide layer may be destroyed by carbon growing in and on the scale [8]. The carburisation lead to fresh internal carbide formation and growth of pre-existing carbide. As carbon activity increases, the conversion of $M_{23}C_6$ to $Cr_2C$ led to rejection of some metallic iron from carbide [9].

Therefore, carburisation resistance can be developed either by (i) adding enough silicon (1.5 - 3 wt.%), to form more or less continuous sublayer of $SiO_2$ beneath the iron oxide layer which is thermodynamically more stable than the iron oxide and is not attacked by carbon, or, by (ii) sulfur which preferentially adsorbs on the surface, and thereby blocks the sites which are otherwise available for the dissociation of hydrocarbon on metal surface, i.e., slows down the carbon transfer to the metal surface [8,10]. Addition of $H_2S/CS_2$ gas stream acts as catalytic poison for decomposition of hydrocarbon (e.g., $CH_4 \rightarrow C + 2H_2$), thereby decreasing the carbon activity and block the ingress of carbon to metallic surface. A certain optimum addition, depending on temperature, suppresses carburisation almost completely, while too much addition has an adverse effect, *i.e.*, sulfidation. Presumably, this addition is at some cost of process efficiency.

## Conclusions

Based on the structural, microstructural and compositional studies conducted on the inside tube wall, the following conclusions can be inferred:

i. There was a breakdown of protective oxide scale which leads to the alteration of subsurface microstructure of base metal at the inner wall of tube.

ii. The carburisation was due to breakdown of protective oxide scale and subsequent ingress of carbon produced by catalytic decomposition of hydrocarbon at base metal substrate. Thick with continuous network of grain boundary carbides as well as fine

intragranular carbides were observed at the advent of carburisation by initiation of pitting.

iii. Carburisation was manifested by the presence of carbides $Cr_2C$ and $M_{23}C_6$ at the subsurface regions.

iv. Phases identified in region "A" (thicker) were; ferrite, magnetite, wustite, $Cr_2C$, $M_{23}C_6$ and carbon soot while in region "B" (thinner), wustite and carbon soot were absent (or present in negligibly small quantity). The different levels of carburisation is caused by inhomogeneous temperature distribution.

v. Catastrophic carburisation (metal dusting corrosion) in region "B" was of uniform metal wastage type whereas in region "A", it was of pitting type.

vi. The failure was due to catastrophic carburisation leading to non-uniform wall thinning.

**ACKNOWLEDGEMENT**

The author is thankful to Mr. B. Ravi Kumar and Mr. Swapan Kumar Das for help rendered in x-ray diffractometry and scanning electron microscopy respectively.

**REFERENCES**

1. T. A. Ramnarayanan and R. Petkovic-Luton, *Proc. 6th Int. Conf. On High Temperature Corrosion*, R. A. Rapp (ed.), NACE, Houston, TX , (1983),430.
2. J. Hemptenmacher, G. Sauthoff and H. J. Grabke, *Werkst. Korros.*, **35**, (1984), 247.
3. M. J. Bennett and J. B. Price, *J. Mat. Sci.*, **16**, (1981), 170.
4. P. A. Lefrancois and W. B. Hoyt, *Corrosion*, **19**, (1963), 360.
5. H. J. Grabke, R. Krajak and J. C. Novapaz, *Corrosion Sci.*, **35**, (1993), 1141.
6. J. H. Devan, "Catastrophic Oxidation of High Temperature Alloys", *Report ORNL-TM-51*, (1961), Oak Ridge National Laboratory, U.S.A.
7. Wolf and H. J. Grabke, *Solid State Commun.*, **54**, (1985), 5.
8. T. A. Ramanarayanan, *Mat. Sci. Engg.*, **87**, (1987), 113.
9. A. Schnaas and H. J. Grabke, *Oxid. Met.*, **12**, (1978), 387.
10. H. J. Grabke, E. M. Petersen and S. R. Srinivasan, *Surf. Sci.*, **67**, (1977), 501.